Application of dilatometric analysis to the study of solid-solid phase transformations in steels

C. García de Andrés, F.G. Caballero, C. Capdevila and L.F. Álvarez

Department of Physical Metallurgy, Centro Nacional de Investigaciones Metalúrgicas (CENIM), Consejo Superior de Investigaciones Científicas (CSIC), Avda. Gregorio del Amo, 8, 28040 Madrid, Spain

Abbreviated Title: Dilatometric analysis in steels

Abstract

This article outlines the use of dilatometry in solid-solid phase transformation research in steel. It describes how dilatometric data are interpreted, with an emphasis on continuous heating and cooling transformation diagrams. These diagrams show the microstructural constituents which result from given heating and cooling conditions, and are an invaluable tool for the metallurgist in characterising steels with respect to their response to heat treatments. Several practical examples and applications of dilatometry in steel research are briefly described in this work.

1. Introduction

Mechanical properties on steels and, therefore, their industrial applications are related to the microstructure. In this sense, the study of all the aspects which can modify the microstructure of the steel during heat treatment is of capital importance. Dilatometry is one of the most powerful techniques for the study of solid-solid phase transformations in steels, because it permits the real time monitoring of the evolution of transformations in terms of dimensional changes occurring in the sample by application of a thermal cycle. It is also one of the classic techniques, along with differential thermal analysis and quantitative analysis of microstructures, most commonly used for determining phase transformation temperatures in steels, both on heating (Ac_1, Ac_3) and cooling (Ar_1, Ar_3). The applicability of dilatometry in phase transformation research is due to the change of the specific volume of a sample during a phase transformation. When a material undergoes a phase change, the lattice structure changes and this is in principle accompanied by a change in specific volume. This technique is widely used to study the transformation behaviour of steels during continuous heating, cooling and isothermal holding. By recording the transformations taking place over a range of conditions, it is possible to present the results in a graphical form, which shows the formation temperatures of microstructural constituents that may be obtained for a given cooling or heating condition. These transformation diagrams are of immense value in metallurgical applications such as heat treatment and welding, and as a means of characterising steels for particular processes.

The aim of this paper is to outline the use of dilatometry in the construction of transformation diagrams such as continuous heating transformation (CHT) and continuous cooling transformation (CCT) diagrams, which are a very useful abacus for steel processing. In this sense, it is appropriate to restate the principles and some special features of the dilatometric analysis. The objective is to give a general appreciation of dilatometry as an experimental

technique vital for the construction of transformation diagrams in the context of the metallurgy of steels.

2. The equipment

Fig. 1 is a scheme of an Adamel Lhomargy DT1000 high-resolution dilatometer which is typical of a modern device for dilatometric analysis. This is fully computer-controlled equipment. The dimensional variations of the specimen are transmitted via an amorphous silica push-rod. These variations are measured by a linear variable differential transformer (LVDT) sensor in a gas-tight enclosure enabling testing under vacuum or in an inert atmosphere to minimise oxidation and/or decarburisation of the specimen during heating to high temperatures. A primary pump enables a vacuum of the order of 10 to 1 Pa being the residual pressure monitored on a dial gauge.

The dilatometer is equipped with a radiation furnace for heating. The heat radiated by two tungsten filament lamps is focussed on the specimen (12 mm in length, 2 mm in diameter) by means of a bi-elliptical reflector. The advantages of this arrangement are the large instantaneous power transfer to a specimen of small mass, and the low thermal inertia, which can be further reduced by using hollow specimens. The temperature is measured with a 0.1 mm diameter type-K Chromel-Alumel thermocouple spot welded to the specimen. Cooling is performed by helium flow directly blow onto the sample surface. The helium flow-rate during cooling is controlled by a proportional servo-valve. If it is desired to cool the specimen below room temperature, this is done using a cryogenic system. In this case, the gas is cooled by passing it through a coil immersed in liquid nitrogen. The excellent efficiency of heat transmission and the very low thermal inertia of the system ensure that the heating and

cooling rates ranging from 0.003 Ks^{-1} to 500 Ks^{-1} remain constant. The dilatometric curve is monitored along the thermal cycle with the help of a computer-assisted electronic device.

3. Phase transformations in steels

Pure iron exists in two crystal forms at atmospheric pressure, one body-centred cubic (bcc) (α-iron) which remain stable from low temperatures up to 910 ºC (the Ae_3 point), when it transforms to a face-centred cubic (fcc) form (γ-iron). The $\alpha \rightarrow \gamma$ transformation during heating is accompanied by an atomic volume change of approximately 1 %, which is associated with a significant contraction on the heating dilatometric curve (relative change in length/temperature trace). This dilatometric feature is shown in Fig. 2 for an ARMCO steel during heating at a rate of 0.05 Ks^{-1} [1].

A study of the constitution and structure of steels must start with the iron-carbon equilibrium diagram. Many of the basic features of this system influence the behaviour of even the most complex alloy steels. There are several temperatures or critical points in the iron-carbon equilibrium diagram which are important, both from the basic and from the practical point-of-view. Firstly, there is the Ae_1 temperature at which the eutectoid reaction occurs, which is 723 ºC in the binary Fe-C diagram. Secondly, there is the Ae_3 temperature when α-iron transforms to γ-iron. For pure iron this occurs at 910 ºC, but the transformation is progressively lowered by the addition of carbon. The Ae_1 and Ae_3 are easily detected by dilatometry during heating or cooling cycles, but some hysteresis is observed. Consequently, three values for each point can be obtained, *Ac* for heating, *Ar* for cooling and *Ae* for equilibrium conditions. It should be emphasised that the *Ac* and the *Ar* values are sensitive to the rates of heating and cooling, as well as to the presence of alloying elements.

The great difference in carbon solubility between γ and α-iron leads normally to the rejection of carbon from the α-phase. The transformation of $\gamma \rightarrow \alpha$ occurs via a eutectoid reaction which plays a dominant role in heat treatment. The eutectoid temperature is 723 ºC and the eutectoid composition is about 0.8 wt-% C. On slowly cooling alloys containing less than 0.80 wt-% C, proeutectoid ferrite is formed from austenite in the range 910-723 ºC with enrichment of the residual austenite in carbon. At 723 ºC, the remaining austenite, now containing 0.8 wt-% carbon, transforms to pearlite, a lamellar mixture of ferrite and iron carbide (cementite). In austenite with 0.80 to 2.06 wt-% C, on slowly cooling in the temperature interval from 1147 to 723 ºC, cementite first forms progressively depleting the austenite in carbon. At 723 ºC, the austenite, containing 0.8 wt-% carbon, transforms to pearlite.

Ferrite, cementite and pearlite are thus the principle constituents of the microstructure of plain carbon steels as they are subjected to relatively slow cooling rates to avoid the formation of metastable phases such as martensite and/or bainite.

Rapid quenching of austenite to room temperature often results in the formation of martensite, a very hard structure in which the carbon, formerly in solid solution in the austenite, remains in solution in the new phase. Unlike ferrite or pearlite, martensite forms by a sudden shear process in the austenite lattice which is not accompanied by atomic diffusion. The martensite reaction in steels occurs during cooling in a temperature range which can be precisely defined for a particular steel. This transformation begins at a martensite start temperature, M_s, which can vary over a wide temperature range from as high as 500 ºC to well below room temperature, depending on the concentration of γ-stabilising alloying elements in the steel. Once M_s is reached further transformation takes place during cooling until the reaction ceases at the M_f temperature. At this temperature all the austenite should have transformed to martensite, but frequently, in practice, a small portion of the austenite does not transform. This is called retained austenite. Large volume fractions of austenite are retained in some

highly alloyed steels, where the M_f temperature is well below room temperature. To obtain the martensitic reaction it is usually necessary for the steel to be rapidly cooled so that the rate of cooling is sufficient to suppress the higher temperature diffusion-controlled ferrite and pearlite reactions, as well as other intermediate reactions such as the formation of bainite.

The fact that the ferrite and pearlite reactions are essentially high temperature transformations occurring between 720 and ~550 ºC and that the formation of martensite is a low temperature reaction, reveals that there is a wide range of intermediate temperature in which neither of these phases forms. This is the region in which fine aggregates of ferrite plates (or laths) and cementite particles are formed. The generic term for this intermediate structure is bainite. Bainite also occurs during continuous cooling at rates too fast for ferrite and pearlite to form, yet not rapid enough to produce martensite.

4. Dilatometric analysis and transformation temperatures

It is the allotropic nature of iron, and its solubility for carbon which makes possible the large range of transformations, microstructures and properties of plain carbon steels. The temperatures at which the transformation of austenite commences and finishes at different rates of cooling, are of importance for planning and designing many industrial processes. Moreover, there are other transformations, which cause the steel to revert to the austenitic condition, in which the knowledge of the transformation temperatures during heating is vital.

4.1. Continuous Heating

The variation of the relative change of length as a function of temperature *($\Delta L/L_0=f(T)$)* shown in the dilatometric curve of Fig. 3, reproduces the contraction undergone by a low carbon steel (Fe-0.11C-0.50Mn) with a ferrite and pearlite initial microstructure during continuous heating. The formation of austenite takes place between the Ac_1 and Ac_3 temperatures which represent, respectively, the temperature at which the ferrite plus pearlite-to-austenite transformation starts and ends.

The transformation start temperature Ac_1 is defined as the temperature at which the linear thermal expansion, graphically represented by the $\Delta L/L_0=f(T)$ function, first deviates from linearity. This behaviour is caused by the volume contraction associated with the austenite formation, which first compensates, and then reverses the normal expansion of the steel due to the increase in temperature. Location of the point at which the deviation occurs is obtained by extrapolating the linear portion of the thermal expansion curve. Likewise, the transformation finish temperature Ac_3 is determinated by extrapolating the linear portion of the curve after transformation.

Normally, no differentiation between the pearlite dissolution process and $\alpha \rightarrow \gamma$ transformation is detected in the heating dilatometric curve. However, the experimental curve in Fig. 3 shows an unusual well-formed contraction associated with the pearlite dissolution [2,3]. Interrupted heating tests at temperatures 10 ºC above and below Ac_1 temperature confirmed that this anomaly effectively corresponds to the pearlite-to-austenite transformation. The possibility to be able to discriminate the pearlite dissolution process and the ferrite-to-austenite transformation by means of high resolution dilatometry permits the determination of the T_C temperature or starting temperature for ferrite-to-austenite transformation. The authors of this paper reported in a previous paper [2] a significant effect of pearlite interlamellar spacing on the dilatometric contraction associated with pearlite dissolution. This effect is caused by the influence of this morphological parameter on the austenite growth rate. An accurate

dilatometric determination of transformation temperatures corresponding to the pearlite dissolution process in these steels could only be performed when fine enough pearlite is obtained. The dilatometric anomaly associated with this transformation is eliminated as pearlite coarsens. The possibility of the accurate identification of the finishing temperature of the pearlite dissolution process makes dilatometric analysis a useful technique for the determination of the most suitable intercritical temperature to obtain dual phase microstructures formed only by ferrite and martensite, widely used in the automobile industry [4].

The small contraction at temperature T_D (Fig. 3), after the relative change in length reaches a minimum, corresponds to the formation of austenite from some grains of ferrite that remains untransformed in the microstructure. As Datta and Gokhale [5] found under isothermal conditions, those residual ferrite grains transform almost instantaneously at the T_D temperature due to a change in ferrite-to-austenite transformation kinetics.

On the other hand, the curves of relative change of length as a function of temperature ($\Delta L/L_0=f(T)$) and its corresponding derivative ($d(\Delta L/L_0)/dt=f(T)$), illustrated in Fig. 4, show the contraction which takes place during the ferrite-to-austenite transformation by continuous heating in a martensitic stainless steel with an initial microstructure of ferrite plus globular carbides ($M_{23}C_6$). These dilatometric curves, apart from $\alpha \rightarrow \gamma$ transformation between Ac_1 and Ac_3 temperatures, reproduce a non-linear length variation associated with the carbide dissolution process. During heating at temperatures above Ac_3, there is a continuous increase of slope in the curve $\Delta L/L_0=f(T)$ which corresponds to the progressive dissolution of the carbides in austenite. The point of inflexion of this section displayed as a maximum in the $d(\Delta L/L_0)/dt=f(T)$ curve corresponds to the A_{cc} temperature or temperature at which the carbide dissolution process ends. Since the presence of carbides in the as-quenched microstructure of these steels has a decisive effect on its wear and corrosion resistance properties, the study of

the carbide dissolution process is important for the optimisation of these materials. In this sense, dilatometric analysis plays an important role in the detection of the temperature at which the carbide dissolution process reaches completion during continuous heating [6].

Once the carbides have been dissolved, austenite presents a significant carbon concentration gradient. As the heating temperature increases, the concentration in the austenite balances out by carbon and carbide-forming elements diffusion, reaching the homogeneity at the A_{ch} temperature. As shown in Fig. 4, dilatometric analysis enables determination of this temperature at the point where the $\Delta L/L_0=f(T)$ curve starts to display again a linear tendency characteristic in the thermal expansion of an homogeneous phase.

4.2. Continuous Cooling

Experimental critical temperatures for the non-isothermal decomposition of austenite into ferrite and pearlite are displayed on the dilatometric curve of a carbon manganese steel (Fe-0.2C-1.1Mn-0.34Si) in Fig. 5. The Ar_3 and Ar_1 critical temperatures correspond, respectively, to the start and finish temperatures of the non-isothermal decomposition of austenite into ferrite plus pearlite. The specific austenite-to-pearlite transformation, may not show a clear indication of the transformation start in many instances. This is not due to lack of resolution, but to a masking of the individual reactions by the continued growth of the other phase. In this case, the pearlite transformation start temperature will be detected by interrupted cooling by quenching experiments and subsequent metallographic examination [7]. In this sense, several quench-out temperatures are selected from cooling dilatometric curves in order to investigate the progress of the austenite→ferrite plus pearlite transformation. Figure 6 shows how the non-isothermal decomposition of austenite occurs in a carbon manganese steel for a cooling rate of 1 Ks^{-1} through micrographs from interrupted cooling samples at different temperatures

of the process. It is clear from Fig. 6a that no transformation has taken place at 765 ºC since the microstructure is formed by martensite and bainite, and no trace of ferrite has been found. Austenite, which does not decompose before the interruption of cooling, transforms to martensite and bainite during quenching. The microstructure from interrupted cooling at Ar_3 temperature (Fig. 6b) shows the first allotriomorphic ferrite grains formed during continuous cooling. That temperature was initially determined from the corresponding cooling dilatometric curve (Fig. 5) and now checked by metallographic analysis. Figures 6c-g show intermediate stages of the reaction. From Fig. 6g it appears that pearlite is formed at around 636 ºC. Finally, Fig. 6h represents a microstructure formed by allotriomorphic ferrite and pearlite similar to that for the non-interrupted cooling test at 1 Ks^{-1} in Fig. 6i. Therefore, at 626 ºC, the transformation has reached completion and this quench-out temperature is the Ar_1 temperature.

By contrast, Fig. 7a shows the dilatometric curve of a low carbon manganese steel (Fe-0.07C-1.56Mn-0.41Si) after rapid cooling (234 Ks^{-1}). Dilatometric analysis indicates that two different transformations take place during cooling in the steel. Metallographic examination shows that the final microstructure obtained after cooling at a rate of 234 Ks^{-1} is composed of bainite and martensite (Fig. 7b). Since bainite is formed at higher temperatures than martensite, there is no doubt that the first volume expansion displayed on the curve corresponds to the transformation of austenite into bainite, whereas the volume expansion shown at the lower temperature corresponds to the transformation of austenite into martensite. Bainite (B_s) and martensite (M_s) transformation start temperatures are, respectively, the temperatures at which the thermal contraction shown by the dilatometric curve deviates from linearity due to the volume expansion associated to the bainite transformation first, and the martensite transformation latter.

On the other hand, Fig. 8 shows a splitting phenomena detected in the martensitic transformation of X30-45Cr13 and X40-60CrMoV14 stainless steels by high resolution dilatometric analysis [8-9]. In these steels, the non-isothermal austenite-to-martensite transformation does not occur continuously in one single stage throughout a certain range of temperatures, M_s-M_f. Under certain conditions, this transformation splits into different and successive stages limited by different points M_{si}. Thus to identify the different splitting stages detected in these steels, M_{sI} is used to represent the temperature at which the principal martensitic transformation (massive austenite-to-martensite) commences. As indicated in the diagram of Fig. 8, the principal martensitic transformation is identified by a minimum in the $\Delta L/L_0=f(T)$ curve. M_{sII} represents the temperature at which the splitting above M_{sI} commences. The weak intensity of this anomaly indicates that it is produced by the transformation of small amounts of austenite and does indeed correspond to the volume increase produced during the martensitic transformation of areas of austenite poor in carbon and carbide-forming elements. This type of splitting is generally explained in terms of carbide precipitation during cooling [8].

Finally, M_{so} represents the temperature at which the splitting below M_{sI} commences. The small expansion anomaly identifying this stage (Fig. 8) indicates that it is also associated with a partial transformation, namely, the martensitic transformation of areas of austenite more concentrated than the massive austenite. This splitting is caused by the concentration gradients produced in the austenite by the diffusion of carbon and carbide-forming elements from the partially or totally dissolved carbides during heating [8]. From stages of austenitization in which the austenite has not reached sufficient levels of homogeneity, either because the carbide dissolution process has not terminated or because the concentration gradients have not been eliminated by solid-state diffusion, the non-isothermal austenite-to-martensite transformation will experience a M_{so}-type splitting.

5. Transformation diagrams

These diagrams are a graphical representation of the temperature and time data concerning the various transformations that occur in a steel by the application of thermal cycles. Although there are two sorts of transformation diagrams, isothermal and non-isothermal, the latter is the clearest and more realistic means of representing industrial processes and treatments. In fact, transformations do not usually occur isothermally in industrial practice, where the cooling and reheating cycles are continuous. Therefore, continuous heating and cooling transformation diagrams provide fundamental insight into the processes that occur in industrial practice, and special attention is devoted to them in this study.

5.1. Continuous Heating Transformation (CHT) Diagrams

To be able to make a rigorous approach to the general study of non-isothermal transformations of austenite, it may be first of all important to determine the actual state of the steel at its austenitisation temperature, specially when the application of different thermal parameters affect the phase transformation processes, the carbide dissolution, and even austenite homogenisation that take place during heating of the material.

Starting from a given initial microstructure, the heating rate and temperature are the two factors that most directly affect the kinetics of the processes developed in the steel. To analyse the effects of these parameters, high-resolution dilatometry is used, and its results are represented in what is generally termed a CHT diagram. Such diagrams are semilogarithmic time-temperature-transformation plots capable of revealing the variation of the critical

temperatures that define the progress of the processes during heating of a steel in real conditions, not in equilibrium.

Figure 9 shows the experimental CHT diagram for a martensitic stainless steel [6]. The range of heating rates studied covers from 0.05 to 2 Ks^{-1}; the former is the rate normally used for determining the critical temperatures, and the latter represents the maximum heating rate used in industry for hardening processes [6]. To know the progress of phase transformation, carbide precipitation and austenite homogenisation, the four above defined critical temperatures (A_{c1}, A_{c3}, A_{cc} and A_{ch}) are determined from dilatometric heating curves for each heating rate tested and superimposed on the corresponding heating curve, plotted as temperature versus log time in the diagram.

Simple observation of this diagram clearly reveals the significant influence of the heating rate on the critical temperatures, specially A_{cc} and A_{ch}, which considerably rise as the heating rate increases. Therefore, the temperature needed for achieving a given austenitising state in the steel must be higher as the process heating rate is increased, and this temperature should not be considered as a treatment parameter depending exclusively on the steel's chemical composition. To disregard the heating rate effect on the austenitisation state is an error that may have major consequences on the final properties of this kind of steel.

5.2. Continuous Cooling Transformation (CCT) Diagrams

CCT diagrams have served an very useful purpose in representing the transformation characteristics of steels not isothermally heat treated, and in revealing the role of alloying elements in influencing the microstructures of the steels. With regard to the decomposition of austenite, these diagrams can be divided, at least, into two separate C-curves, one of which

represents reconstructive transformations (ferrite and pearlite) and the other, displacive reactions (such as bainite) [10].

Construction of CCT diagrams is performed as follows: once the transformation start and finish reaction temperatures have been determined for each cooling rate, these temperatures are superimposed on the corresponding cooling curve, which is plotted as temperature versus log time. In conjunction with metallographic evaluation of the microstructure, the reaction boundaries are drawn in, connecting the transformation temperatures with curves. Vickers results for each sample may also help with the metallographic analysis.

In these diagrams, it is important to state the prior austenite grain diameter (PAGD), which has a significant effect on the different phase transformation kinetics. The effect of the prior austenite grain size on continuous cooling transformations is explained by the nucleation of softer constituents, such as ferrite and pearlite, which takes place primarily at the grain boundaries. If the grain size is coarsened, there is a reduction in grain boundary area, and therefore the nucleation capacity of ferrite and pearlite is also reduced. As the reconstructive transformations are retarded, the displacive transformations are enhanced.

CCT diagrams for a medium carbon microalloyed forging steel (Fe-0.4C-1.4Mn-0.2Mo-0.1V) with two different prior austenite grain diameters (PAGD) are shown in Fig. 10 [11]. In these diagrams, F is ferrite, P is pearlite, B is bainite and M is martensite. Note that dotted lines have been used to indicate reaction boundaries where their position lies somewhere between cooling curves, and thus cannot be drawn in with certainty. From this figure, it is evident that the ferrite and pearlite formation areas shift to higher times as the austenite grain size increases. Ferrite is obtained after decomposition of austenite with a PAGD of 12 μm by continuous cooling at every tested cooling rate, whereas for a PAGD of 68 μm, ferrite is only formed at cooling rates lower than 30 Ks^{-1}. Moreover, pearlite appears for a PAGD of 12 μm at cooling rates lower than 1.5 Ks^{-1}. However, for a PAGD of 68 μm, pearlite is obtained

cooling down at rates lower than 0.6 Ks^{-1}. On the other hand, the anisothermal austenite-to-bainite transformation for a PAGD of 12 μm occurs at cooling rates higher than 0.12 Ks^{-1} in this steel. For a PAGD of 68 μm, this transformation takes place at cooling rates ranging from 30 to 0.07 Ks^{-1}. Therefore, the bainite formation region is reduced and shifted to lower cooling rates as the PAGD increases.

6. Modelling of dilatometric behaviour of austenite formation during continuous heating

Gone are the days when industry could simply make a whole matrix of alloys, test them, and then hope for the best. Such methods are unacceptable in the modern competitive environment. This realisation has caused a great increase in research leading to the development of thermodynamic and kinetic models which help to reduce the time and expense of alloy development, and maintain the enormous success of steel as a structural material. Since the dimensional changes detected by dilatometry are related to the volume fraction of transformation, dilatometric analysis can also be used to validate phase transformation models [1,3,12]. The purpose of this section is to show a method for quantitatively relating length change to the extent of transformation for the particular case of non-isothermal austenite formation.

Assuming that the sample expands isotropically, the change of the sample length ΔL referred to the initial length L_o at room temperature is related to volume change ΔV and initial volume V_o at room temperature for small changes as follows:

$$\frac{\Delta L}{L_o} = \frac{V - V_o}{3V_o} \tag{1}$$

Therefore, $\frac{\Delta L}{L_o}$ can be calculated from the volumes of the unit cells and the volume fractions of the different phases present in the microstructure at every temperature during continuous heating:

$$\frac{\Delta L}{L_o} = \frac{1}{3}\left[\frac{\left(2V_\alpha\ a_\alpha^3 + \frac{1}{3}V_\theta\ a_\theta\ b_\theta\ c_\theta + V_\gamma\ a_\gamma^3\right) - \left(2V_{\alpha_o} a_{\alpha_o}^3 + \frac{1}{3}V_{\theta_o} a_{\theta_o} b_{\theta_o} c_{\theta_o}\right)}{\left(2V_{\alpha_o} a_{\alpha_o}^3 + \frac{1}{3}V_{\theta_o} a_{\theta_o} b_{\theta_o} c_{\theta_o}\right)}\right] \quad (2)$$

being V_{α_o,θ_o} the initial volume fraction of ferrite and cementite, respectively, present in the microstructure at room temperature. Likewise, $V_{\alpha,\theta,\gamma}$ are the volume fraction of ferrite, cementite and austenite, respectively, at any transformation temperature. The austenite volume fraction is calculated at every temperature using a kinetic model described elsewhere [3,12]. The factors 2 and 1/3 in equation (2) are due to the fact that, the unit cell of ferrite and cementite contain 2 and 12 iron atoms, respectively, whereas that of austenite has 4 atoms. Moreover, a_{α_o} is the lattice parameter of ferrite at room temperature, taken to be that of pure iron (a_{α_o} = 2.866 Å); a_{θ_o}, b_{θ_o}, c_{θ_o} are the lattice parameters of cementite at room temperature [13] given by 4.5246, 5.0885 and 6.7423 Å, respectively; and a_{γ_o} is the lattice parameter of austenite at room temperature as a function of the chemical composition of the austenite [14,15]:

$$a_{\gamma_o} = 3.573 + 0.033C + 0.00095Mn - 0.0002Ni + 0.0006Cr + 0.0031Mo + 0.0018V \quad (3)$$

where the chemical composition is measured in wt-% and a_{γ_o} is in Å.

Likewise, a_α, a_θ, b_θ, c_θ, and a_γ are the lattice parameters of ferrite (α), cementite (θ) and austenite (γ) at any transformation temperature. They are calculated as follows:

$$a_\alpha = a_{\alpha_o}\left[1+\beta_\alpha\,(T-300)\right] \tag{4a}$$

$$a_\gamma = a_{\gamma_o}\left[1+\beta_\gamma\,(T-300)\right] \tag{4b}$$

$$a_\theta = a_{\theta_o}\left[1+\beta_\theta\,(T-300)\right] \tag{4c}$$

$$b_\theta = b_{\theta_o}\left[1+\beta_\theta\,(T-300)\right] \tag{4d}$$

$$c_\theta = c_{\theta_o}\left[1+\beta_\theta\,(T-300)\right] \tag{4e}$$

where $\beta_{\alpha,\theta,\gamma}$ are the linear thermal expansion coefficients of ferrite, cementite and austenite, respectively, in K^{-1}. The values of the linear thermal expansion of ferrite and austenite [16] considered in these calculations were $\beta_\alpha = 1.244\times10^{-5}$ K^{-1} and $\beta_\gamma = 2.065\times10^{-5}$ K^{-1}. Moreover, the thermal expansion coefficient of cementite increases with temperature [13]. Using data published by Stuart and Ridley [13], the expression for the linear expansion coefficient as a function of temperature is:

$$\beta_\theta = 6.0\times10^{-6} + 3.0\times10^{-9}(T-273) + 1.0\times10^{-11}(T-273)^2 \tag{5}$$

where T is the temperature in K.

The dilatation curve calculated using equation (2) for a eutectoid steel with a fully pearlitic initial microstructure and heated at a rate of 0.05 Ks^{-1} is shown in Fig. 11 in comparison with the experimental result [12].

The calculated relative change in length is consistent with the measured value at every temperature. Experimental critical temperatures, Ac_1 and Ac_3, as well as the magnitude of the overall contraction due to austenite formation are accurately reproduced by the calculated dilatation curve.

7. Conclusions

Dilatometry is a powerful tool for the characterisation and study of solid-solid phase transformations in steels. The construction of CHT and CCT diagrams from dilatometric data allows the prediction of microstructure for given rates of heating and cooling, respectively. Finally, a method has been provided for quantitatively relating the relative length change to the volume fraction of transformation. That method makes dilatometric analysis a useful technique to validate phase transformation theoretical models.

Acknowledgements

The authors acknowledge financial support from the European Coal and Steel Community (ECSC-7210. EC/939) and the Spanish Comisión Interministerial de Ciencia y Tecnología (CICYT-MAT95-1192-CE). F.G. Caballero would like to thank the Consejería de Educación, D.G. de Investigación de la Comunidad Autónoma de Madrid (CAM) for the financial support in the form of a Postdoctoral Research Grant.

References

1. F.G. Caballero, C. Capdevila, and C. García de Andrés, Kinetics and Dilatometric Behaviour of Non-Isothermal Ferrite-to-Austenite Transformation, *Materials Science and Technology* 17: 1114-1118 (2001).
2. C. García de Andrés, F.G. Caballero, and C. Capdevila, Dilatometric Characterization of Pearlite Dissolution in 0.1C-0.5Mn Low Carbon Low Manganese, *Scripta Materialia* 38: 1835-1842 (1998).
3. F.G. Caballero**,** C. Capdevila, and C. García de Andrés, Modelling of kinetics of austenite formation in steels with different initial microstructures, *ISIJ International* 41: 1093-1102 (2001).
4. G. Krauss, *Steels: Heat Treatment and Processing Principles*, ASM International, Ohio, p. 274 (1989).
5. D.P. Datta and A.M. Gokhale, Austenitization kinetics of pearlite and ferrite aggregates in a low carbon steel containing 0.15 wt pct C, *Metallurgical and Materials Transactions A* 12A: 443-450 (1981).
6. C. Garcia, L.F. Alvarez, and M. Carsi, Effects of heat treatment parameters on non-equilibrium transformations and properties of X45Cr13 and X60Cr14MoV martensitic stainless steels, *Welding International* 6: 612-621 (1992).
7. F.G. Caballero, C. Capdevila, and C. García de Andrés, Evaluation and review of the simultaneous transformation model in HSLA steels, *Materials Science and Technology*, *in press.*
8. C. García de Andrés, J.A. Jiménez, and L.F. Álvarez, Splitting phenomena occurring in the martensitic transformation of Cr13 and CrMoV14 stainless steels in the absence of

carbide precipitation, *Metallurgical and Materials Transactions A* 27A: 1799-1805 (1996).

9. C. García, L.F. Alvarez, and M. Carsí, *Interest of Dilatometric Analysis in the Study of Structural Transformations of Martensitic Stainless Steels,* Proc. Int. Conf. On MatTech'90, Espoo, Finland (June 10-18, 1990).
10. H.K.D.H. Bhadeshia, *Bainite in Steels*, The Institute of Materials, London, p. 33 (1992).
11. C. García de Andrés, C. Capdevila, F.G. Caballero, and D. San Martín, Effect of Molybdenum on Continuous Cooling Transformations in Three Medium Carbon Forging Steels, *Journal of Materials Science* 36: 565-571 (2001).
12. C. García de Andrés, F.G. Caballero, C. Capdevila, and H.K.D.H. Bhadeshia, Modelling of Kinetics and Dilatometric Behaviour of Non-Isothermal Pearlite-to-Austenite Transformation in an Eutectoid Steel, *Scripta Materialia* 39: 791-796 (1998).
13. H. Stuart and N. Ridley, Thermal expansion of cementite and other phases, *Journal of the Iron and Steel Institute* 204: 711-717 (1966).
14. N. Ridley, H. Stuart, and L. Zwell, Lattice parameters of Fe-C austenites at room temperature, *Trans. of A.I.M.E.* 245: 1834-1836 (1969).
15. D.J. Dyson and B. Holmes, Effect of alloying additions on the lattice parameter of austenite, *Journal of the Iron and Steel Institute* 208: 469-474 (1970).
16. M. Takahashi, Reaustenitization from Bainite in Steels, Ph.D. Thesis, University of Cambridge, Cambridge, UK (1992).

Fig. 1. General diagram of dilatometer.

Fig. 2. Heating dilatation curve of an ARMCO steel (Fe-0.002C-0.05Mn) obtained at a heating rate of 0.05 Ks^{-1}.

Fig. 3. Heating dilatation curve of a low carbon steel (Fe-0.11C-0.50Mn) obtained at a heating rate of 0.05 Ks^{-1}.

Fig. 4. Diagram of the heating dilatometric response of $\alpha \rightarrow \gamma$ transformation and the carbide dissolution process of martensitic stainless steels.

Fig. 5. Cooling dilatometric curve of a carbon manganese steel (Fe-0.20C-1.1Mn-0.34Si) obtained at a cooling of 1 Ks^{-1}.

Fig. 6. Optical micrographs corresponding to the evolution of ferrite and pearlite formation during cooling at a rate of 1 Ks^{-1} in a carbon manganese steel (Fe-0.20C-1.1Mn-0.34Si). Quench-out temperatures: (a) 765 ºC; (b) 758 ºC (Ar_3); (c) 754 ºC; (d) 746 ºC; (e) 726 ºC; (f) 676 ºC; (g) 636 ºC; (h) 626 ºC (Ar_1); (i) room temperature.

Fig. 7. (a) Cooling dilatometric curve and (b) microstructure of a low carbon manganese steel (Fe-0.07C-1.56Mn-0.41Si) after cooling at a rate of 234 Ks^{-1}.

Fig. 8. Dilatometric representation of the splitting phenomena in the martensitic transformation of Cr13 and CrMoV14 stainless steels.

Fig. 9. Continuous heating transformation diagram for a X45Cr13 martensitic stainless steel.

Fig. 10. Continuous cooling transformation diagrams of a medium carbon microalloyed forging steel (Fe-0.4C-1.4Mn-0.2Mo-0.1V) with a PAGD of (a) 12 μm and (b) 68 μm.

Fig. 11. Calculated and experimental dilatation curve of a eutectoid steel heated at a rate of 0.05 Ks^{-1}.

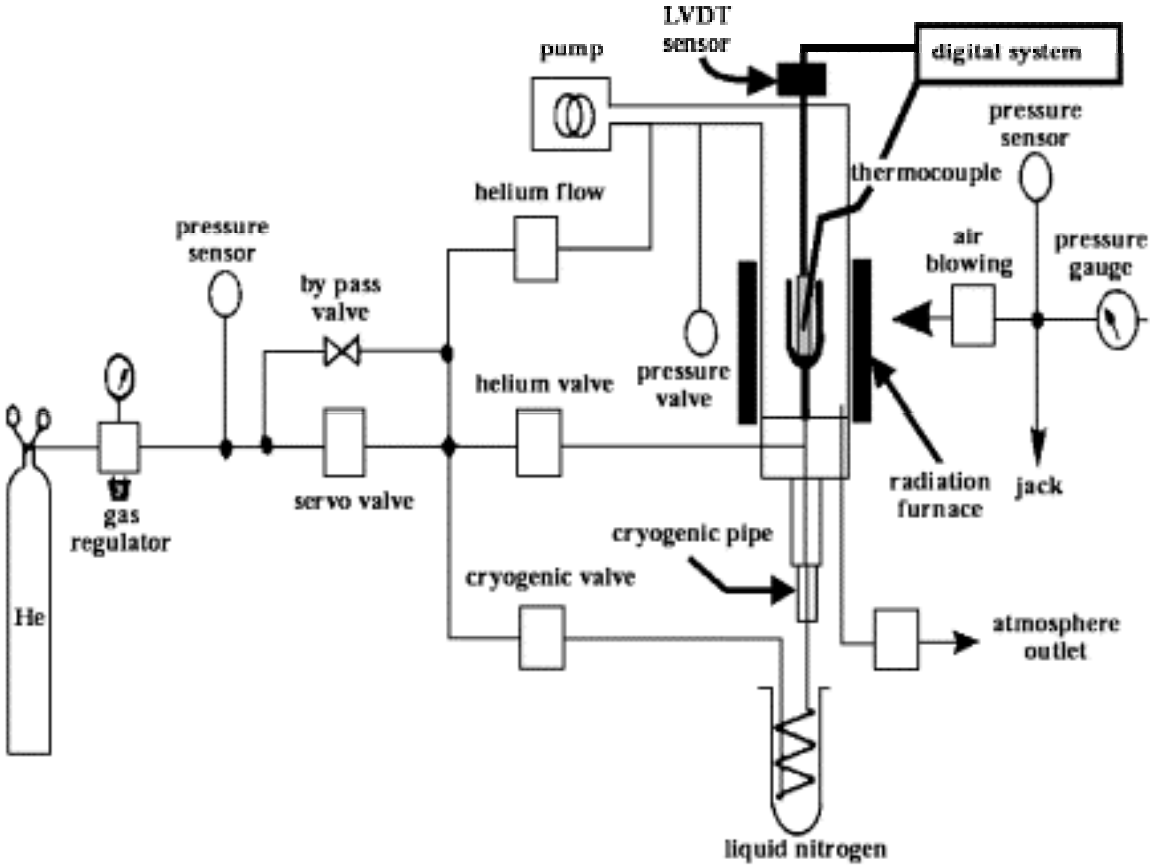

Fig. 1. General diagram of dilatometer.

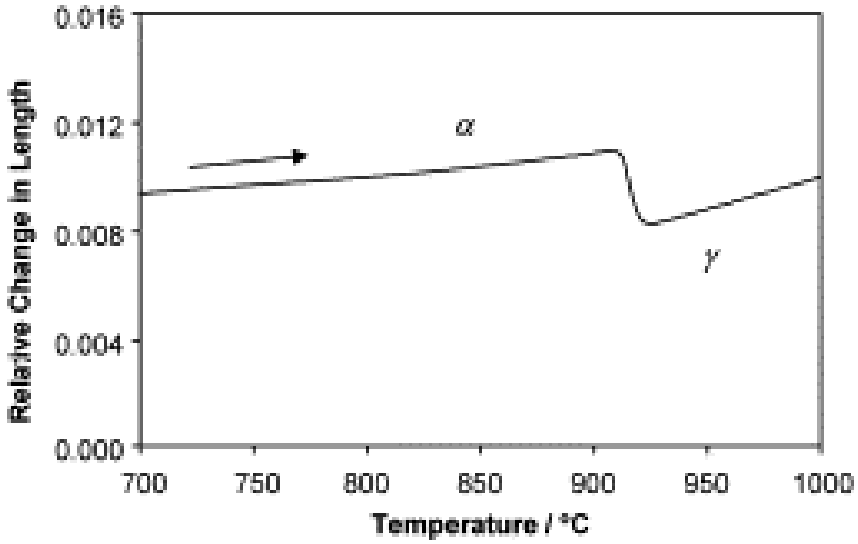

Fig. 2. Heating dilatation curve of an ARMCO steel (Fe–0.002C–0.05Mn) obtained at a heating rate of 0.05 K s^{-1}.

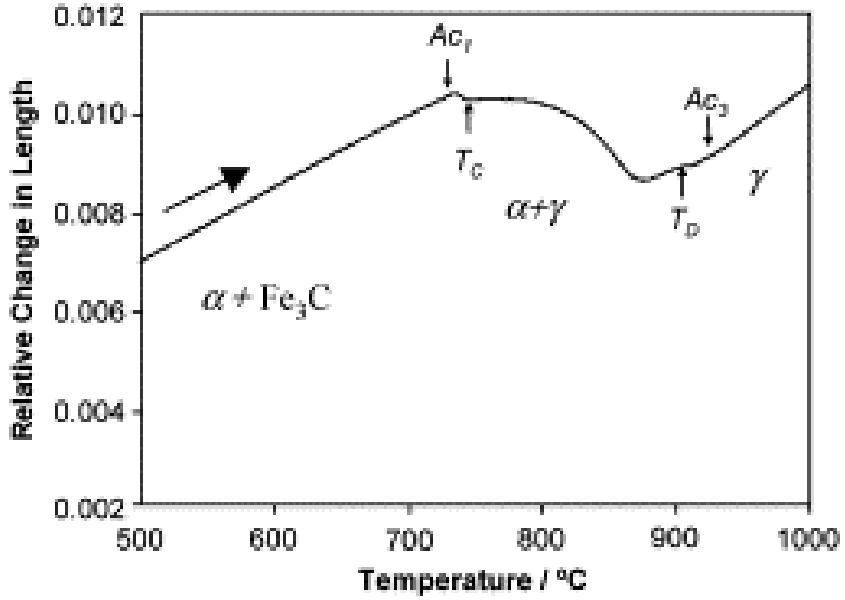

Fig. 3. Heating dilatation curve of a low carbon steel (Fe–0.11C–0.50Mn) obtained at a heating rate of 0.05 K s^{-1}.

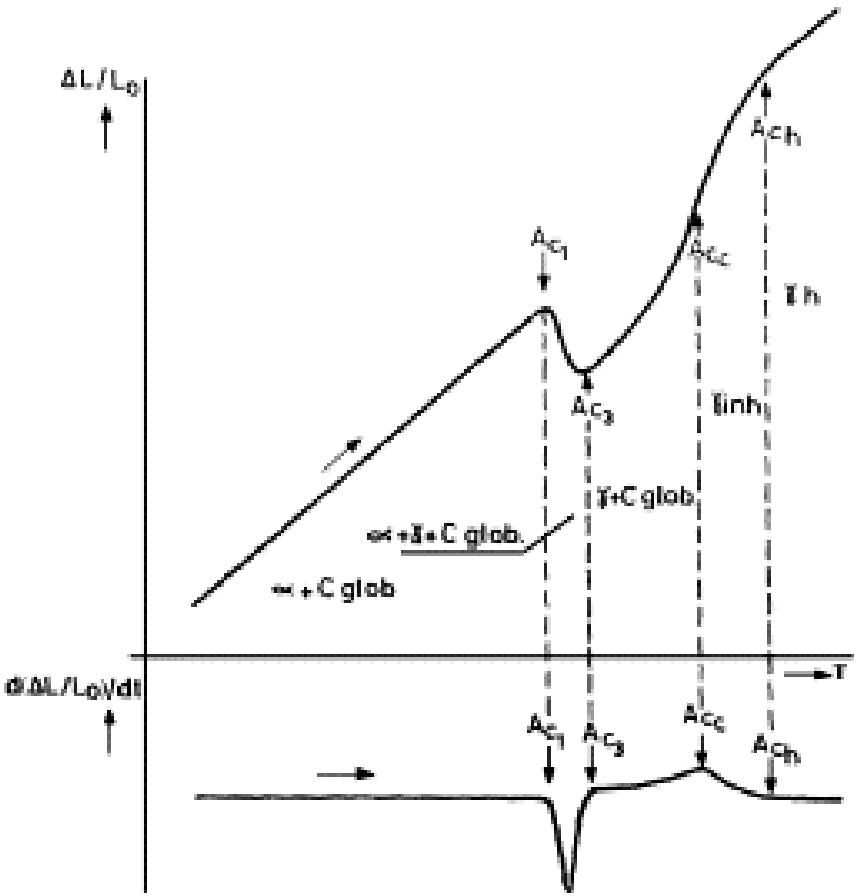

Fig. 4. Diagram of the heating dilatometric response of α→γ transformation and the carbide dissolution process of martensitic stainless steels.

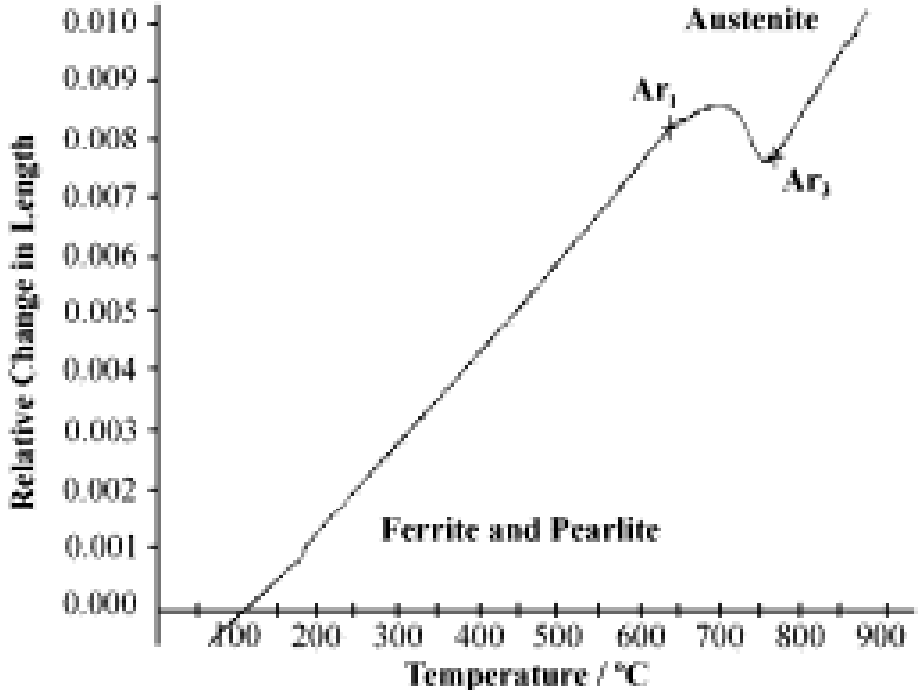

Fig. 5. Cooling dilatometric curve of a carbon manganese steel (Fe–0.20C–1.1Mn–0.34Si) obtained at a cooling of 1 K s^{-1}.

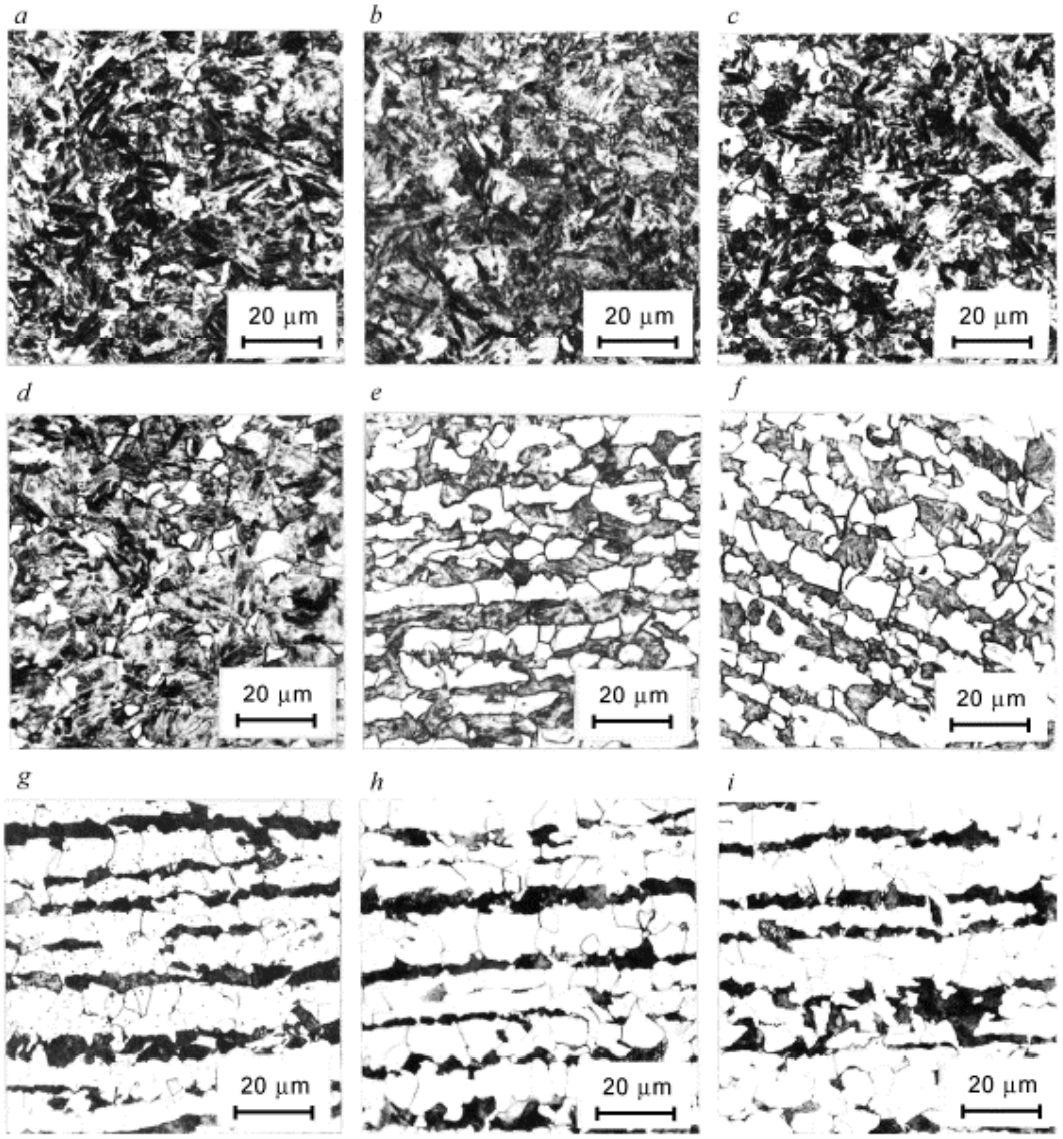

Fig. 6. Optical micrographs corresponding to the evolution of ferrite and pearlite formation during cooling at a rate of 1 K s^{-1} in a carbon manganese steel (Fe–0.20C–1.1Mn–0.34Si). Quench-out temperatures: (a) 765 °C; (b) 758 °C (A_{r3}); (c) 754 °C; (d) 746 °C; (e) 726 °C; (f) 676 °C; (g) 636 °C; (h) 626 °C (A_{r1}); (i) room temperature.

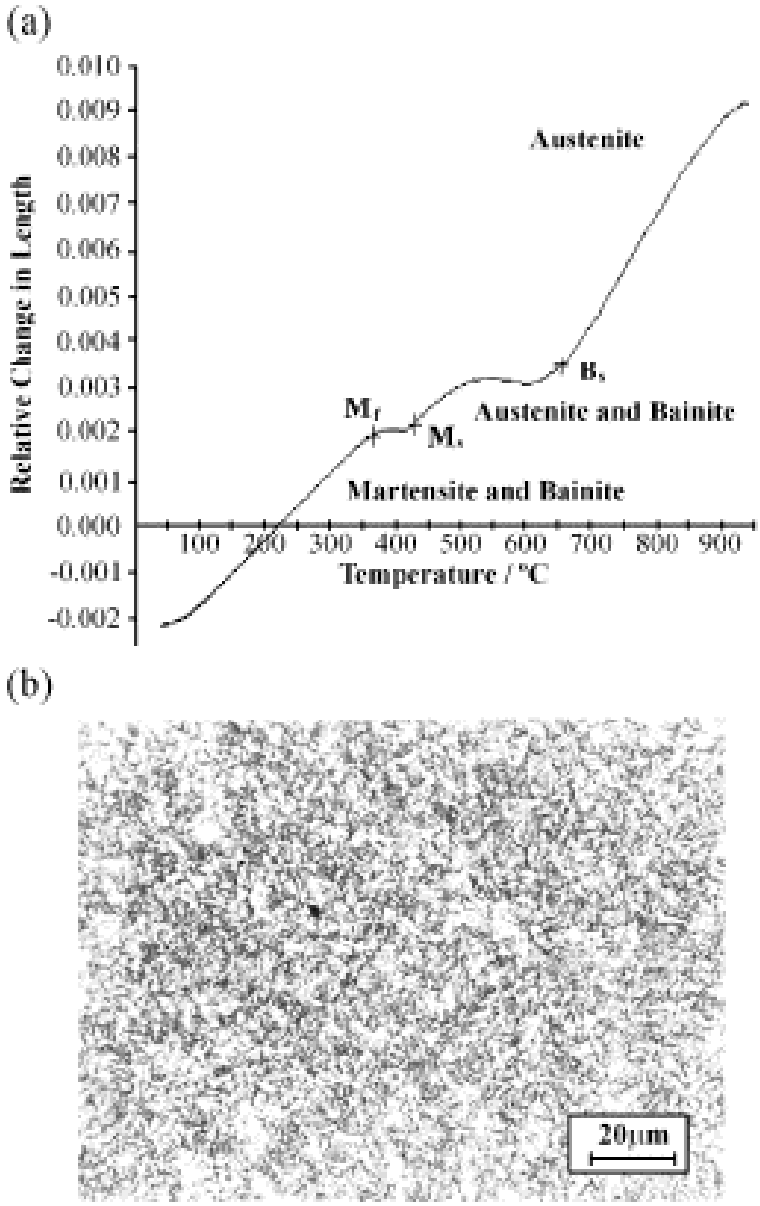

Fig. 7. (a) Cooling dilatometric curve and (b) microstructure of a low carbon manganese steel (Fe–0.07C–1.56Mn–0.41Si) after cooling at a rate of 234 K s^{-1}.

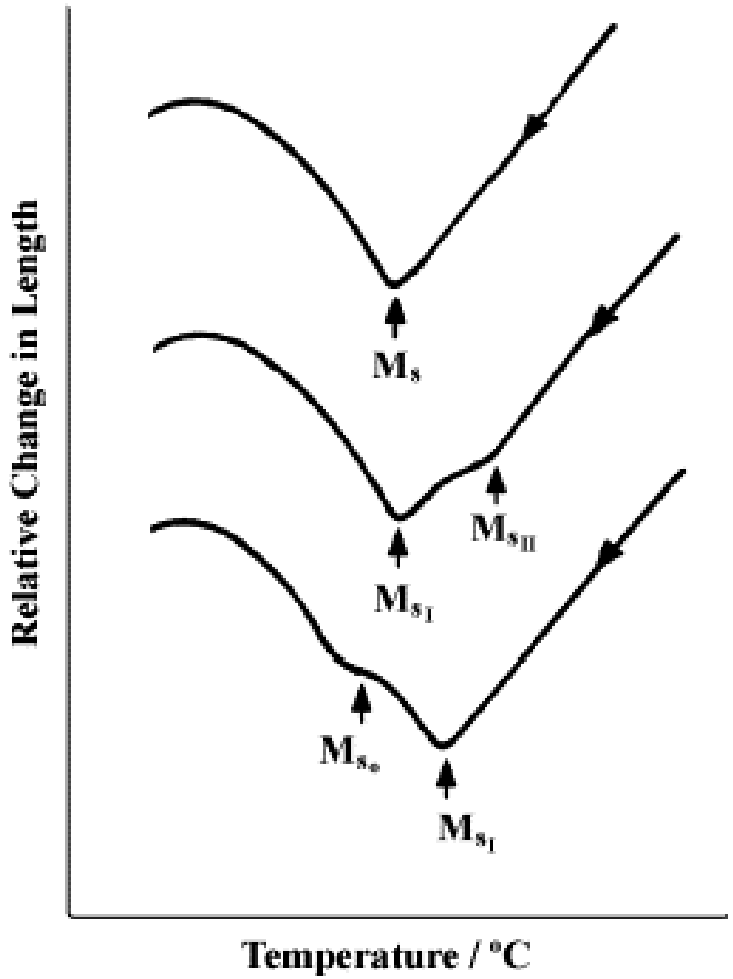

Fig. 8. Dilatometric representation of the splitting phenomena in the martensitic transformation of Cr13 and CrMoV14 stainless steels.

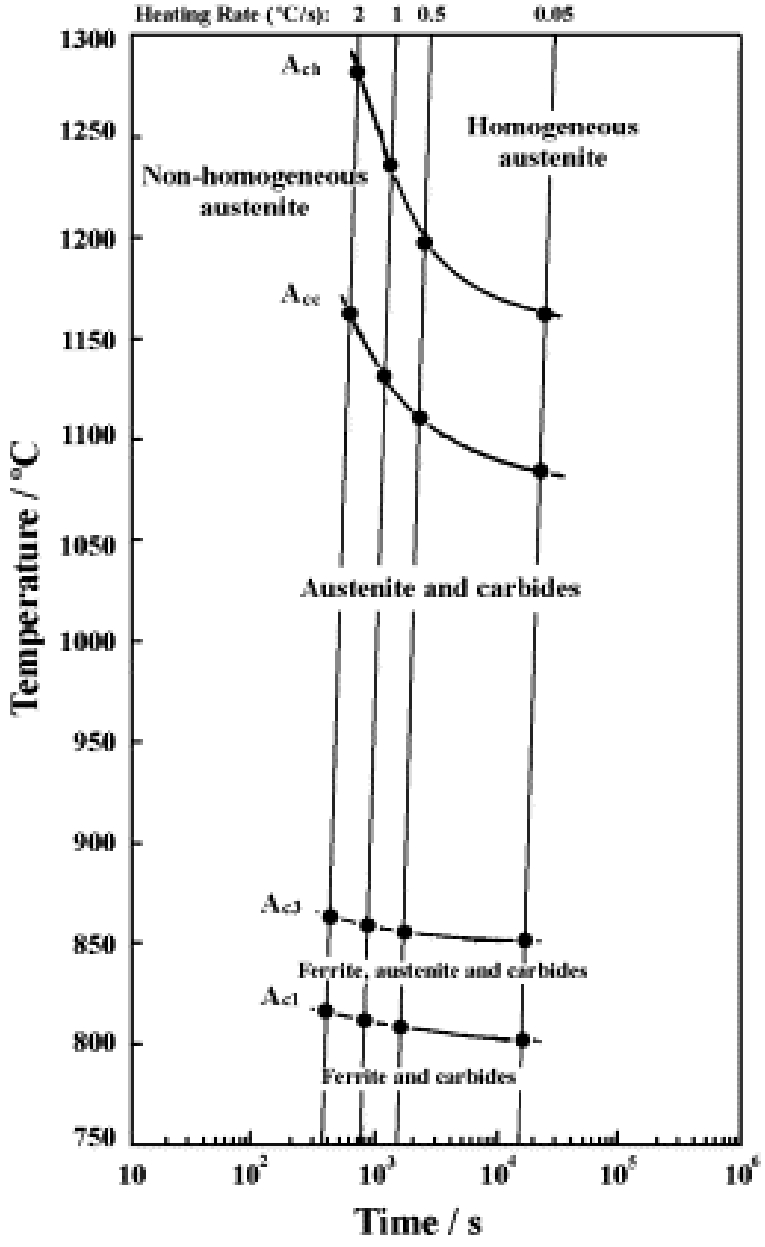

Fig. 9. CHT diagram for a X45Cr13 martensitic stainless steel.

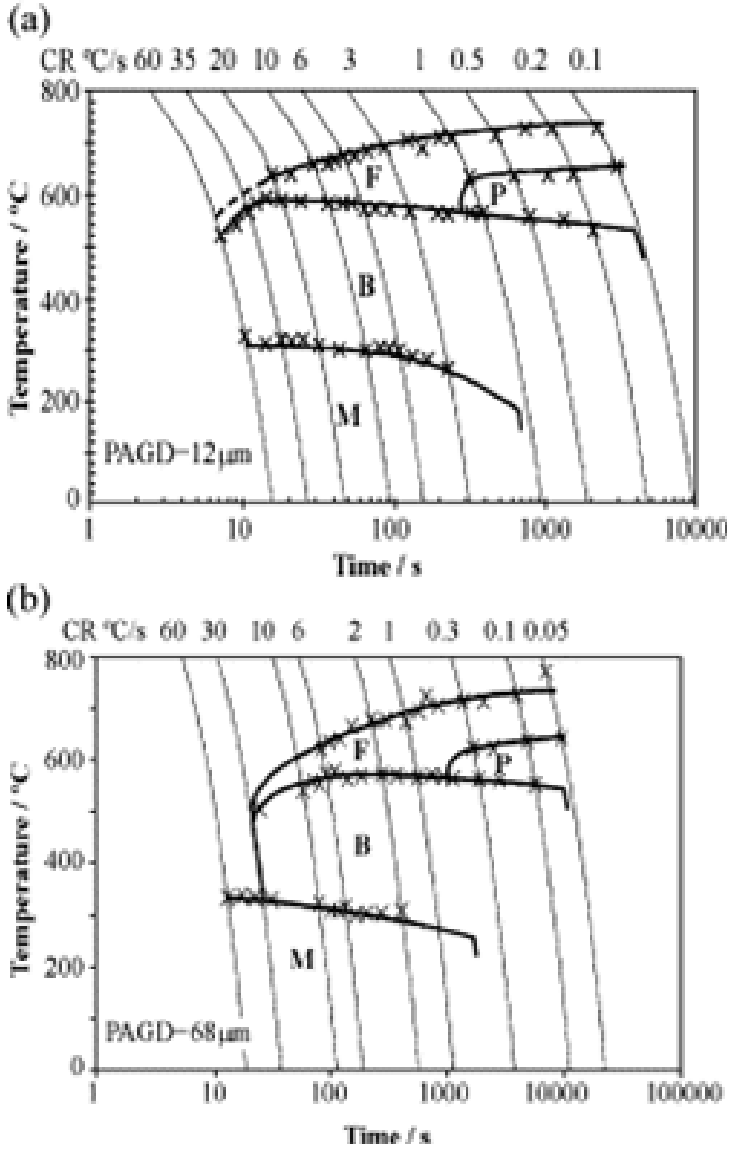

Fig. 10. CCT diagrams of a medium carbon microalloyed forging steel (Fe–0.4C–1.4Mn–0.2Mo–0.1V) with a PAGD of (a) 12 and (b) 68 μm.

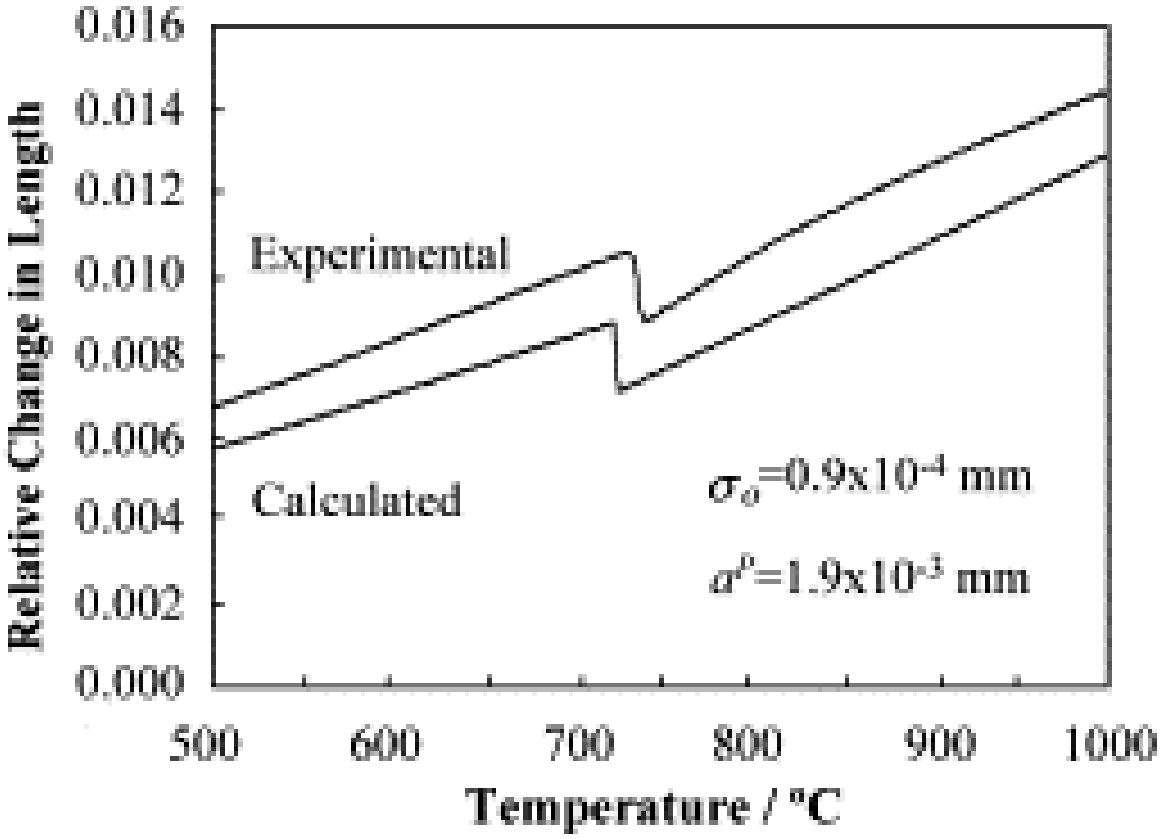

Fig. 11. Calculated and experimental dilatation curve of a eutectoid steel heated at a rate of 0.05 K s^{-1}.